Matched slow optical soliton pairs via biexciton coherence in quantum dots

Wen-Xing Yang,[1,2,*] Ai-Xi Chen,[3,4] Ray-Kuang Lee,[2] and Ying Wu[5]

[1]*Department of Physics, Southeast University, Nanjing 210096, China*

[2]*Institute of Photonics Technologies, National Tsing-Hua University, Hsinchu 300, Taiwan*

[3]*Centre for Atom Optics and Ultrafast Spectroscopy, Swinburne University of Technology, Melbourne 3122, Australia*

[4]*Department of Applied Physics, School of Basic Science, East China Jiaotong University, Nanchang 330013, China*

[5]*Wuhan National Laboratory for Optoelectronics and School of Physics, Huazhong University of Science and Technology, Wuhan 430074, China*

(Received 18 February 2011; published 28 July 2011)

We theoretically investigate the simultaneous formation and stable propagation of slow optical soliton pairs in semiconductor quantum dots with a four-level biexciton-exciton cascade configuration. Owing to the destructive interference set up by two continuous wave control fields that couple to a biexciton state, the linear as well as nonlinear dispersion can be dramatically enhanced simultaneously with the absorptions of two weak probe fields being almost suppressed. These results reveal that the detrimental distortions of the two weak-pulsed probe fields due to dispersion effects can be well balanced by the self-phase modulation effect under very low input light intensity, which leads to the slow temporal optical soliton pairs with matched group velocity and amplitude. We also show that the propagation of slow optical solitons can be strongly modified by the biexciton coherence.

DOI: 10.1103/PhysRevA.84.013835 PACS number(s): 42.65.Tg, 42.50.Gy, 78.67.Hc

I. INTRODUCTION

Optical solitons refer to a special kind of optical fields that propagate undistorted over a long distance and remain unaffected after the collision with each other in nonlinear media. Such a remarkable propagation effect has been the subject of intense theoretical and experimental studies from nonlinear optics [1,2], matter waves [3], and microcavities [4,5] due to their potential applications in information processing and communication. The formation of temporal optical solitons, first observed in optical fiber, is the consequence of the balance between nonlinearity and dispersion. However, conventional optical soliton generation required high-powered lasers since the nonlinear effect in passive media (optical fibers, for example) is extremely weak. As a result, optical solitons generated in this way generally travel with group velocity very close to the speed of light in vacuum and, thus, long propagation distance is needed.

To access slow lights, in the past few years, considerable attention has been paid to the study of optical propagation via electromagnetically induced transparency (EIT) in resonant atomic systems, in which an on-resonance excitation scheme is used [6]. Based on the striking features under weakly driven EIT conditions [7–15], the possibility of generating slow optical solitons has been explored recently [16–22]. Because of their robust nature with a slow propagating velocity, the slow optical solitons may have the potential to be promising candidates of well-characterized, distortion-free optical pulses and, hence, have important technological applications in optical and telecommunication engineering.

It should be noted that the tremendous success of EIT studies in resonant atomic systems has stimulated considerable experimental and theoretical efforts in extending these studies to semiconductor devices. Many approaches for realizing EIT in semiconductor devices have been proposed theoretically and reported experimentally [23–29]. One of the important motivations comes from mature semiconductor manufacturing technologies [30–44], for which the interaction between semiconductor devices and optical light fields is strongly enhanced in comparison with atomic systems due to the achievable large dipole moments [45]. Nonlinear optical experiments can be performed with pulses of a few hundreds of femtoseconds, which are long compared to the inhomogeneous broadening but short enough so that the electron-phonon interaction, which acts on a picosecond time scale, can be neglected [46–48], offering time scales necessary for coherent interaction.

Recently, we have studied the slow optical soliton formations and the dispersion management of optical solitons in GaAs/$Al_xGa_{1-x}As$ semiconductor structure [49–51]. For slow-light solitons in semiconductor structures, only one probe field is used and, hence, one obtains a single nonlinear Schrödinger equation (NLSE) that admits a single soliton under the condition where the dispersion effect can be balanced by the self-phase modulation (SPM) effect. However, one often encounters propagation of multiple fields in a single medium for technical applications. In this paper, we show the simultaneous formation and stable propagation of slow optical soliton pairs in semiconductor quantum dots (SQD) with a four-level biexciton-exciton cascade configuration. We show that the absorption of the two weak-pulsed probe fields can be almost suppressed while, simultaneously, the nonlinearity is enhanced due to the destructive interference set up by two continuous wave (cw) control fields that couple to a biexciton state. By employing the density operator formalism for describing the interaction of the system, we also demonstrate that the SPM effects can balance the dispersion and result in the slow temporal optical soliton pairs with matched group velocity and amplitude. More interestingly, the propagation of slow optical solitons can be strongly modified by the biexciton coherence.

*wenxingyang2@126.com

This paper is arranged as follows. In the next section, we give the description of the system and solutions in the linear regime. In Sec. III, by taking the reasonable and realistic approximate conditions, we derive the system's NLSE describing the envelope's evolution of two weak-pulsed probe fields. Then, optical soliton pair solutions with matched group velocity and amplitude in the system are provided and their stability and controllability during propagation are discussed in detail. At the end of this paper, we conclude with a brief discussion and conclusion in Sec. IV.

II. DESCRIPTION OF THE SYSTEM AND THE SOLUTIONS IN THE LINEAR REGIME

By referring to experimental demonstration of SQD samples [52,53], the device we consider here may be a GaAs/Al_xGa_{1-x}As semiconductor structure with 15 periods of 17.5-nm GaAs layer and 25-nm $Al_{0.3}Ga_{0.7}$ barriers, grown by molecular beam epitaxy. The GaAs layer samples can be held at 10 K in a helium flow cryostat. The samples were etched to remove the GaAs substrate layer and allow transmission. As shown schematically in Fig. 1, the ground state $|0\rangle$, one-exciton states $|1\rangle$, $|2\rangle$, and biexciton state $|3\rangle$ resemble a four-level cascade configuration. The value of the biexciton binding energy ΔE is several meV [54]. In the present system, two pulsed probe fields ($p1$, $p2$) with angular frequencies $\omega_{p1,p2}$, one-half Rabi frequencies $\Omega_{p1,p2}$, and two continuous wave coherent couple fields ($c1$, $c2$) with angular frequency $\omega_{c1,c2}$, one-half Rabi frequency $\Omega_{c1,c2}$, complete the respective excitations. In this system, the exciton coherence is the nonradiative coherence, which can lead to destructive interference in the optical transition between the one-exciton and bound biexciton states. The electric-field vector for the probe and couple fields can be written as $\mathbf{E}_{j=p1,p2,c1,c2} = \Sigma_j \mathbf{e}_j \mathcal{E}_j \exp[i(\mathbf{k}_j\mathbf{r} - \omega_j t)] + \text{c.c.}$,

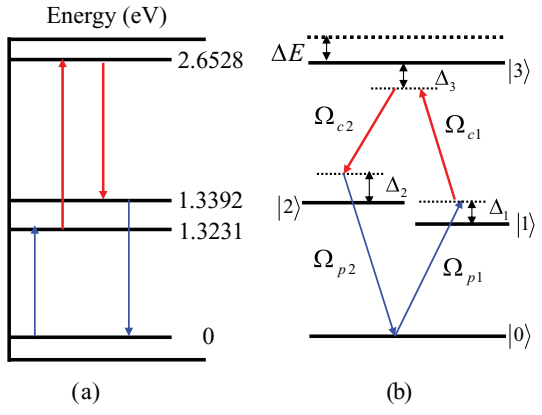

FIG. 1. (Color online) (a) The energy-level diagram for the investigated GaAs/Al_xGa_{1-x}As SQD. (b) The schematic of the corresponding energy levels and transitions in the SQD. The SQD sample with four levels interacts with two cw laser control fields coupling, respectively, $|1\rangle \leftrightarrow |3\rangle$ and $|2\rangle \leftrightarrow |3\rangle$ (angular frequencies $\omega_{c1,c2}$ and Rabi frequencies $2\Omega_{c1,c2}$) and two pulsed probe fields driving the transition $|0\rangle \leftrightarrow |1\rangle$ and $|0\rangle \leftrightarrow |2\rangle$ (angular frequencies $\omega_{p1,p2}$ and Rabi frequencies $2\Omega_{p1,p2}$).

where $\mathbf{k}_j$, $\mathcal{E}_j$, and $\mathbf{e}_j$ are wave vector, envelope amplitudes, and polarization direction of the jth probe or control fields, respectively, and c.c. represents complex conjugate. The time evolution of the system, expressed using the density operator ρ, is governed by the Liouville equation which, under the electric-dipole and rotating-wave approximations, leads to the following equations for the density matrix elements ρ_{ij}:

$$\dot{\rho}_{11} = -\gamma_{1l}\rho_{11} + i\Omega_{p1}^*\rho_{01} - i\Omega_{p1}\rho_{10} + i\Omega_{c1}^*\rho_{31} - i\Omega_{c1}\rho_{13}, \tag{1}$$

$$\dot{\rho}_{22} = -\gamma_{2l}\rho_{22} + i\Omega_{p2}^*\rho_{02} - i\Omega_{p2}\rho_{20} + i\Omega_{c2}^*\rho_{32} - i\Omega_{c2}\rho_{23}, \tag{2}$$

$$\dot{\rho}_{33} = -\gamma_{3l}\rho_{33} + i\Omega_{c2}\rho_{23} - i\Omega_{c2}^*\rho_{32} + i\Omega_{c1}\rho_{13} - i\Omega_{c1}^*\rho_{31}, \tag{3}$$

$$\dot{\rho}_{10} = id_1\rho_{10} + i\Omega_{p1}\rho_{00} + i\Omega_{c1}^*\rho_{30} - i\Omega_{p2}\rho_{12} - i\Omega_{p1}\rho_{11}, \tag{4}$$

$$\dot{\rho}_{20} = id_2\rho_{20} + i\Omega_{p2}\rho_{00} + i\Omega_{c2}^*\rho_{30} - i\Omega_{p2}^*\rho_{20} - i\Omega_{p1}\rho_{21}, \tag{5}$$

$$\dot{\rho}_{30} = id_3\rho_{30} + i\Omega_{c1}\rho_{10} + i\Omega_{c2}\rho_{20} - i\Omega_{p2}\rho_{32} - i\Omega_{p1}\rho_{31}, \tag{6}$$

$$\dot{\rho}_{32} = id_4\rho_{32} - i\Omega_{c2}^*\rho_{33} + i\Omega_{c2}^*\rho_{22} - i\Omega_{c1}^*\rho_{21} + i\Omega_{p2}^*\rho_{03}, \tag{7}$$

$$\dot{\rho}_{21} = id_5\rho_{21} - i\Omega_{p1}\rho_{20} - i\Omega_{c1}\rho_{23} + i\Omega_{c2}^*\rho_{31} + i\Omega_{p2}^*\rho_{01}, \tag{8}$$

$$\dot{\rho}_{31} = id_6\rho_{31} + i\Omega_{p1}^*\rho_{03} + i\Omega_{c1}^*\rho_{33} - i\Omega_{c2}^*\rho_{12} - i\Omega_{c1}^*\rho_{11}, \tag{9}$$

with $\rho_{ij} = \rho_{ji}^*$, $d_1 = \Delta_1 + i\gamma_1$, $d_2 = \Delta_2 + i\gamma_2$, $d_3 = \Delta_3 + i\gamma_3$, $d_4 = (\Delta_3 - \Delta_1) + i\gamma_4$, $d_5 = (\Delta_1 - \Delta_2) + i\gamma_5$, and $d_6 = (\Delta_1 - \Delta_3) + i\gamma_6$. γ_j ($j = 1,2,3$) denotes the total decay rate of exciton and biexciton coherence, which are added phenomenologically in the above density matrix equations (1)–(9). In SQDs, the overall decay rate is given by $\gamma_1 = \gamma_{1l} + \gamma_{10}^d$, $\gamma_2 = \gamma_{2l} + \gamma_{20}^d$, $\gamma_3 = \gamma_{3l} + \gamma_{30}^d$, $\gamma_4 = (\gamma_{2l} + \gamma_{3l} + \gamma_{23}^d)$, $\gamma_5 = (\gamma_{2l} + \gamma_{1l} + \gamma_{21}^d)$, and $\gamma_6 = (\gamma_{3l} + \gamma_{1l} + \gamma_{31}^d)$. The former γ_{jl} denotes the lifetime broadening linewidth, which is due primarily to longitudinal optical photon emission at low temperature. The latter γ_{ij}^d is the dephasing broadening linewidth, which may originate from electron-electron scattering, electron-phonon scattering, as well as inhomogeneous broadening due to scattering on interface roughness. Generally, γ_{ij}^d is the dominant mechanism in a semiconductor solid-state system in contrast to the atomic systems. $\Delta_j = \omega_{pj} - (\omega_j - \omega_0)$ ($j = 1,2$) and $\Delta_3 = \omega_{pj} + \omega_{cj} - (\omega_3 - \omega_0)$ are the one- and two-photon detunings, respectively ($\hbar\omega_j$ is the energy of the states $|j\rangle$). A more complete theoretical treatment taking into account coherent nonlinear optical processes for the dephasing rates induced by Coulomb correlations is thought to be interesting,

but beyond the scope of this paper. The effects of Coulomb correlations on coherent nonlinear optical processes have been investigated extensively in earlier studies and can be described by microscopic theories based on dynamics controlled truncation schemes and also on the use of N-exciton many-body eigenstates [55–58]. We would rather take phenomenological values (available from earlier experiments) for the dephasing rates here since we are interested in showing applications of the this SQD system as an efficient device for generating optical solitons. We stress that the above phenomenological model to the interaction of the electromagnetic fields with the semiconductor structure has proven to be well suited to modeling quantitatively experimental results [23–25,32].

The electric-field evolution is governed by the Maxwell equation

$$\nabla^2\mathbf{E} - \frac{1}{c^2}\frac{\partial^2\mathbf{E}}{\partial t^2} = \frac{1}{\varepsilon_0 c^2}\frac{\partial^2\mathbf{P}}{\partial t^2}, \tag{10}$$

with

$$\mathbf{P} = N\sum_{j=1,2}\mu_{0j}\rho_{j0}\exp[i(\mathbf{k}_{pj}\cdot\mathbf{r}-\omega_{pj}t)] + \mu_{3j}\rho_{j3}\exp[i(\mathbf{k}_{cj}\cdot\mathbf{r}-\omega_{cj}t)] + \text{c.c.} \tag{11}$$

being the electric polarization intensity, where N, c, μ_{ij}, and ε_0 are the concentration, velocity of light in vacuum, electric-dipole matrix element associated with the transition from $|j\rangle$ to $|i\rangle$, and vacuum dielectric constant, respectively, and $\mathbf{k}_{pj} = \mathbf{k}_j - \mathbf{k}_0$ and $\mathbf{k}_{cj} = \mathbf{k}_j - \mathbf{k}_3$. Under the slowly varying envelope approximation [59], the Maxwell equation can be reduced to the first-order equation. Thus, we can obtain the slowly varying envelope equation for describing the two probe fields evolution

$$\frac{\partial\Omega_{p1}(z,t)}{\partial z} + \frac{1}{c}\frac{\partial\Omega_{p1}(z,t)}{\partial t} = i\kappa_{01}\rho_{10}, \tag{12}$$

$$\frac{\partial\Omega_{p2}(z,t)}{\partial z} + \frac{1}{c}\frac{\partial\Omega_{p2}(z,t)}{\partial t} = i\kappa_{02}\rho_{20}, \tag{13}$$

where $\kappa_{0j} = N\Omega_{pj}|\mathbf{e}_{pj}\cdot\mu_{0j}|^2/(2\varepsilon_0\hbar c)$ $(j = 1,2)$. For simplicity, we have assumed $\mathbf{k}_{pj} = \mathbf{e}_z k_{pj}$.

In order to provide a clear picture of the interplay between the dispersion and nonlinear effects of the SQD system interacting with four optical fields, we must solve Eqs. (4)–(6) and (12) and (13). Before solving these nonlinearly equations, let us first examine the linear excitations of the system, which may provide useful hints of the weak nonlinear theory developed in the next section. To this aim, we assume that the Rabi frequencies $2\Omega_{p1,p2}$ of the pulsed probe fields are much smaller than those of the couple fields $2\Omega_{c1,c2}$, and electrons initially populated the energy level $|0\rangle$ (i.e., $\rho_{00} \simeq 1$). Then, under the perturbation expansion $\rho_{ij} = \Sigma_k\rho_{ij}^{(k)}$, where $\rho_{ij}^{(k)}$ is the kth-order part of ρ_{ij} in terms of $\Omega_{p1,p2}$, it can be shown that $\rho_{ij}^{(0)} = 0$ $(i \neq j)$ and $\rho_{11}^{(k)} = \rho_{22}^{(k)} = \rho_{33}^{(k)} = 0$. Considering the first order of the pulsed probe fields and taking time Fourier transform of Eqs. (4)–(9) and (12) and (13),

$$\rho_{ij}^{(1)}(t) = \frac{1}{\sqrt{2\pi}}\int_{-\infty}^{\infty}\beta_{ij}^{(1)}(\omega)e^{-i\omega t}d\omega, \quad i,j = 0,1,2,3 \tag{14}$$

$$\Omega_k(t) = \frac{1}{\sqrt{2\pi}}\int_{-\infty}^{\infty}\Lambda_k(\omega)e^{-i\omega t}d\omega, \quad k = p1,p2 \tag{15}$$

with ω being the Fourier transform variable, we have

$$(\omega+d_1)\beta_{10}^{(1)} + \Lambda_{p1} + \Omega_{c1}^*\beta_{30}^{(1)} = 0, \tag{16}$$

$$(\omega+d_2)\beta_{20}^{(1)} + \Lambda_{p2} + \Omega_{c2}^*\beta_{30}^{(1)} = 0, \tag{17}$$

$$(\omega+d_3)\beta_{30}^{(1)} + \Omega_{c1}\beta_{10}^{(1)} + \Omega_{c2}\beta_{20}^{(1)} = 0, \tag{18}$$

$$\beta_{32}^{(1)} = \beta_{21}^{(1)} = \beta_{31}^{1} = 0, \tag{19}$$

$$\frac{\partial\Lambda_{p1}}{\partial z} - i\frac{\omega}{c}\Lambda_{p1} = i\kappa_{01}\beta_{10}, \tag{20}$$

$$\frac{\partial\Lambda_{p2}}{\partial z} - i\frac{\omega}{c}\Lambda_{p2} = i\kappa_{02}\beta_{20}. \tag{21}$$

The solutions to Eqs. (16)–(18) are given by

$$\beta_{10}^{(1)} = \frac{\Omega_{c1}^*\Omega_{c2}\Lambda_{p2} - D_{c2}(\omega)\Lambda_{p1}}{D(\omega)}, \tag{22}$$

$$\beta_{20}^{(1)} = \frac{\Omega_{c1}\Omega_{c2}^*\Lambda_{p1} - D_{c1}(\omega)\Lambda_{p2}}{D(\omega)}, \tag{23}$$

$$\beta_{30}^{(1)} = -\frac{(\omega+d_2)\Omega_{c1}\Lambda_{p1} + (\omega+d_1)\Omega_{c2}\Lambda_{p2}}{D(\omega)}, \tag{24}$$

with $D_{c1}(\omega) = |\Omega_{c1}|^2 - (\omega+d_1)(\omega+d_3)$, $D_{c2}(\omega) = |\Omega_{c2}|^2 - (\omega+d_2)(\omega+d_3)$, and $D(\omega) = |\Omega_{c1}|^2(\omega+d_2) - |\Omega_{c2}|^2(\omega+d_1) - (\omega+d_1)(\omega+d_2)(\omega+d_3)$. Here, β_{ij} and $\Lambda_{a,b,c}$ are the Fourier transforms of ρ_{ij} and $\Omega_{p1,p2}$, respectively. With the help of Eqs. (22)–(24), Eqs. (20) and (21) can be solved analytically, yielding

$$\Lambda_{p1}(z,\omega) = \frac{\Lambda_{p1}(0,\omega)[W^+(\omega)\exp(izK^-) - W^-(\omega)\exp(izK^+)] - \Lambda_{p2}(0,\omega)[\exp(izK^-) - \exp(izK^+)]}{W^+(\omega) - W^-(\omega)}, \tag{25}$$

$$\Lambda_{p2}(z,\omega) = \frac{\Lambda_{p2}(0,\omega)[W^+(\omega)\exp(izK^+) - W^-(\omega)\exp(izK^-)] + W^+(\omega)W^-(\omega)\Lambda_{p1}(0,\omega)[\exp(izK^-) - \exp(izK^+)]}{W^+(\omega) - W^-(\omega)}, \tag{26}$$

with

$$K^{\pm}(\omega) = \frac{\omega}{c} + \frac{-[\kappa_{01}D_{c2}(\omega) + \kappa_{02}D_{c1}(\omega)] \pm G(\omega)}{2D(\omega)}, \tag{27}$$

$$W^{\pm}(\omega) = \frac{\kappa_{01}D_{c2}(\omega) - \kappa_{02}D_{c1}(\omega) \pm G(\omega)}{2\kappa_{01}\Omega_{c1}^*\Omega_{c2}}, \tag{28}$$

where $G(\omega) = \sqrt{[\kappa_{01}D_{c2}(\omega) - \kappa_{02}D_{c1}(\omega)]^2 + 4\kappa_{01}\kappa_{02}|\Omega_{c1}|^2|\Omega_{c2}|^2}$. $\Lambda_{p1,p2}(0,\omega)$ are the initial conditions for two pulsed probe fields at the entrance of the SQD structure $z = 0$. There exist two modes (the $K^{\pm}$ modes) described by the linearized dispersion relations $K = K^+(\omega)$ and $K = K^-(\omega)$,

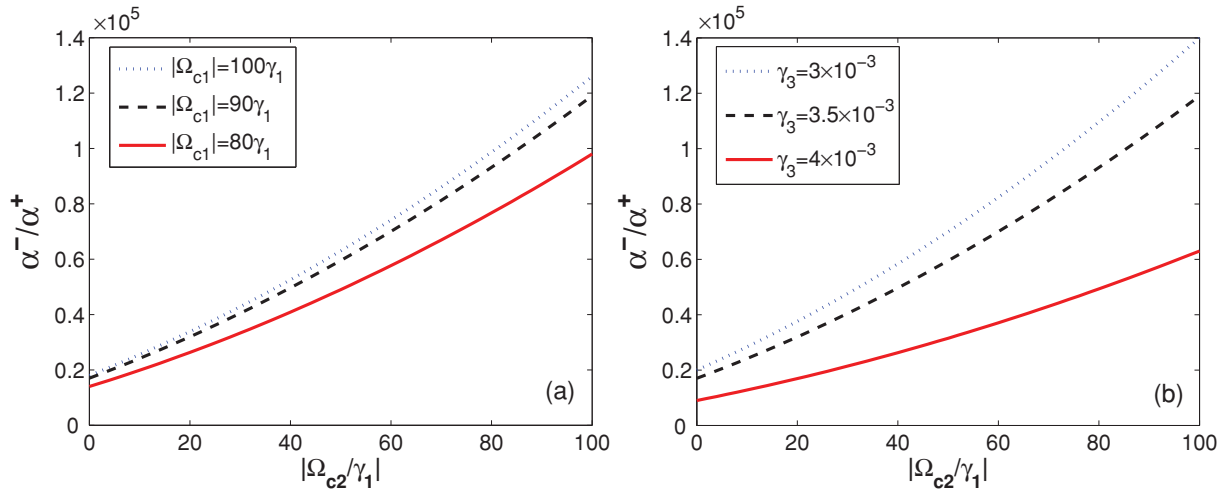

FIG. 2. (Color online) The ratio of the absorption coefficients α^-/α^+ for the two different modes versus the amplitude $|\Omega_{c2}|$ of the cw control field $c2$ (a) for several different amplitudes $|\Omega_{c1}|$ with $\gamma_3 = 3.5 \times 10^{-3}\gamma_1$ and for (b) the different decay rates for biexciton coherence γ_3 with $|\Omega_{c1}| = 90\gamma_1$. The other parameter values are $\kappa_{01} = \kappa_{02} = 3.4 \times 10^6$ cm^{-1} meV, $\gamma_1 = \gamma_2 = 0.054$ meV, $\Delta_1 = 3.1\gamma_1$, $\Delta_2 = 12\gamma_1$, and $\Delta_3 = -0.05\gamma_1$.

respectively. In most operation conditions, they can be expanded into a rapid conversion power series around the center frequencies $\omega_{p1,p2}$ of the pulse probe fields; that is, $\omega = 0$. We thus have

$$K^{\pm}(\omega) = K_0^{\pm} + K_1^{\pm}\omega + \tfrac{1}{2}K_2^{\pm}\omega^2 + \mathcal{O}(\omega^3), \tag{29}$$

where $K_j^{\pm} = (\partial^j K^{\pm}/\partial\omega^j)|\omega = 0\,(j = 0,1,2)$ give the dispersion coefficients in different orders. Generally, $\alpha^{\pm} = \mathrm{Im}[K_0^{\pm}]$ and $\mathrm{Re}[K_0^{\pm}]$ represent the phase shifts per unit and absorption coefficients, respectively. The group velocities ($V_g^{\pm}$) of the $K^{\pm}$ modes are given by $1/\mathrm{Re}[K_1^{\pm}]$. The group-velocity dispersion can be described by $\mathrm{Re}[K_2^{\pm}]$, which results in the spreading of the pulsed probe fields as the distance z increases. By applying an inverse Fourier transform to $\Lambda_{p1,p2}$,

$$\Omega_{p1,p2}(z,t) = \frac{1}{\sqrt{2\pi}}\int_{-\infty}^{\infty}\exp(-i\omega t)\Lambda_{p1,p2}(z,\omega)d\omega, \tag{30}$$

we can achieve the linearized results of pulsed probe fields

$$\Omega_k(z,t) = \Omega_k^{(+)}(z,t) + \Omega_k^{(-)}(z,t), \quad k = p1,p2 \tag{31}$$

$$\Omega_{p1}^{(\pm)}(z,t) = F^{\pm}\left(t - \frac{z}{V_g^{(\pm)}}\right)\exp[iK_0^{\pm}z], \tag{32}$$

$$\Omega_{p2}^{(\pm)}(z,t) = W^{\pm}(0)\Omega_p^{(\pm)}(z,t), \tag{33}$$

with

$$F^{\pm} = \frac{\pm\Omega_{p2}(0,t) \mp W^{\mp}(0)\Omega_{p1}(0,t)}{W^{+}(0) - W^{-}(0)} \tag{34}$$

and $W^{\pm,\mp}(0) = W^{\pm,\mp}|_{\omega=0}$. It can be seen from Eqs. (31)–(34) that, when the given input fields $\Omega_{p1,p2}(0,t)$ satisfy the condition $\Omega_{p2}/\Omega_{p1} = W^{\pm,\mp}(0)$ leading to $F^{\pm,\mp} \equiv 0$, there exists no $K^{\mp}$ mode excitation, and the two pulsed probe fields in the SQD medium are $\Omega_{p1}(z,t) = \Omega_{p1}(0,t - z/V_g^{\pm})\exp[iK_0^{\pm}z]$ and $\Omega_{p2}(z,t) = W^{\pm}\Omega_{p1}(z,t)$. Even in the situation where we use only one input, i.e., $\Omega_{p2}(0,0) = 0 \to \Omega_{p2}(0,t)/\Omega_{p1}(0,t) \neq W^{\pm}$, both K^+ and K^- modes will simultaneously be excited in the SQD medium. This requires that a multiple-single-channel-induced-transparency based four-wave-mixing (FWM) process be operative. However, there exist parameter regimes in which the absorption coefficients $2\alpha^{\pm} = 2\mathrm{Im}[K_0^{\pm}]$ differ significantly from each other, and one of the modes always decays much faster than the other. Thus, we can only consider a single-mode excitation by neglecting a short propagation distance.

For the temperatures up to 10 K, the electric density kept below 4×10^{18} cm^{-3}, the typical parameters for $GaAs/Al_xGa_{1-x}As$ QDs can be chosen as $\gamma_{jd} = 50$ μeV, $\gamma_{jl} = 4.1$ μeV, $\mu_{j0} = 1 \times 10^{-16}$ esu cm; as a result, we can obtain $\gamma_j = 0.054$ meV, $\kappa_{0j} = 3.4 \times 10^6$ cm^{-1} meV ($j = 1,2$). In addition, we choose $\Delta_1 = 3.1\gamma_1$, $\Delta_2 = 12\gamma_1$, and $\Delta_3 = -0.05\gamma_1$. Under small biexciton decoherence conditions, Fig. 2 plots the absorption coefficients ratio $\alpha^-/\alpha^+ = \mathrm{Im}[K_0^-]/\mathrm{Im}[K_0^+]$ versus the amplitude $|\Omega_{c2}|$ for several different amplitude values of another cw control field [see Fig. 2(a)] and different decay rates for biexciton coherence γ_3 [see Fig. 2(b)] in this biexciton-exciton cascade configuration. It is clearly seen that the absorption coefficient ratio increases as the amplitudes of the two cw control fields increase, and the absorption coefficients satisfy $\alpha^- \gg \alpha^+$ as shown in Fig. 2, which illustrates the K^- mode decay more quickly than the K^+ mode, thus, we can safely neglect the K^- mode after a short characteristic propagation distance. These results are the behavior of multiphoton quantum destructive interference between the two different excitation channels: coupling excitation channel and back-coupling excitation channel. Physically, when the probe field Ω_{p2} is the same intensity, an efficient back-coupling excitation channel to one-exciton state $|1\rangle$ becomes important (i.e., $|0\rangle \to |1\rangle$ mediated by the biexciton state $|3\rangle$ via $\Omega_{p2} + \Omega_{c2}^* + \Omega_{c1}^*$), which is π out of phase with respect to the coupling excitation channel $|0\rangle \to |1\rangle$ provided by Ω_{p1}. These processes lead to simultaneous suppression of amplitudes of one-exciton states

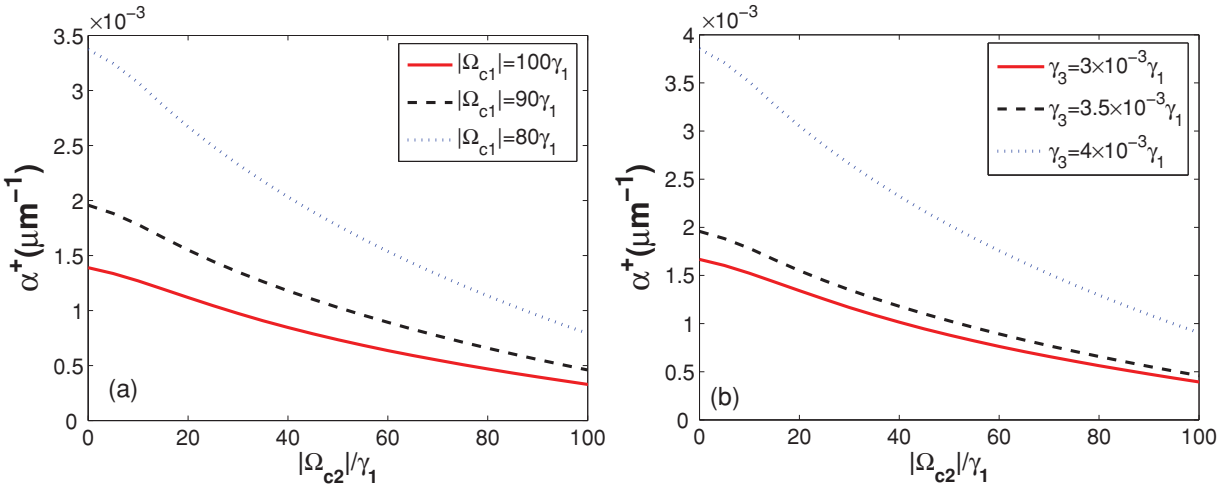

FIG. 3. (Color online) Absorption coefficient α^+ versus the amplitude $|\Omega_{c2}|$ of the cw control field $c2$ (a) for several different amplitude values of another cw control field $|\Omega_{c1}|$ with $\gamma_3 = 3.5 \times 10^{-3}\gamma_1$ and for (b) the different decay rates for biexciton coherence γ_3 with $|\Omega_{c1}| = 90\gamma_1$. The other parameters are the same as in Fig. 2.

$|1\rangle$ and $|2\rangle$ from multiphoton destructive interference through the two pathways that connect each of the two states. This is an important difference between the destructive interference mediated by the biexciton coherence and the conventional EIT process, where the destructive interference resulting from it occurs between two one-photon channels. As a consequence, the two weak-pulsed probe fields propagate with the matched group velocity $V_g = V_g^+$.

In Fig. 3, we plot the absorption coefficient α^+ as a function of the amplitude $|\Omega_{c2}|$ [see Fig. 3(a)] of the cw control field $c2$ for several different amplitude values $|\Omega_{c1}|$ of another cw control field $c1$ and different decay rates for biexciton coherence γ_3 [see Fig. 3(b)]. Figure 3 shows that the amplitudes of absorption coefficients are in the order of 10^{-4} μm^{-1}, and the absorption can be largely suppressed under appropriate conditions in this four-level SQD system. The suppression of the exciton absorption can, in principle, arise from destructive interference induced by a biexciton coherence. This is analogous, but by no means equivalent, to EIT in atomic systems since, in our case, the nonradiative coherence is induced via interactions between excitons [55,60]. Figures 2(b) and 3(b) illustrate this point, and from Figs. 2 and 3, one can find that the absorption coefficient α^+ can be modified not only by the amplitude of the cw control fields, but also by the biexciton coherence. We should note that the biexciton decoherence rates γ_3 have been assumed much less than the exciton decoherence rate $\gamma_{1,2}$, i.e., $3 \times 10^{-3}\gamma_1 \sim 4 \times 10^{-3}\gamma_1$. Within current experimental technology, the characteristic biexciton lifetimes $1/\gamma_3$ of SQD are typically longer than a few nanoseconds, and numerous observations also indicate that the biexciton lifetime may reach values of 10 ns or even higher [61,62]. Here, a larger biexciton decoherence rate can lead to more pronounced absorption as shown in Figs. 2(b) and 3(b).

It should be noted that Eq. (27) is obtained in the linear regime of the system under the weak-field and adiabatic approximations while ignoring the higher-order terms of probe fields. In order to preserve shapes of the two pulsed probe fields, we need to include SPM, which may balance the spread effect due to the group-velocity dispersion described by the K_2^+ coefficients to generate a pair of matched optical solitons. In the next section, we will explore the higher-order terms of $\Omega_{p1,p2}$ while systematically keeping terms up to ω^2 in Eq. (29) for the purpose of demonstrating the formation of temporal optical soliton pairs in the four-level SQD system.

III. NONLINEAR DYNAMICS AND MATCHED OPTICAL SOLITON PAIRS

We now discuss the nonlinear evolution of the two pulse probe fields in the situation that the K^- mode decays very quickly and can be neglected after a very short propagation distance as shown in Fig. 2. The pulsed probe field Ω_{p1} under these conditions has the form

$$\Omega_{p1}(z,t) = \Omega_{p1}^{(+)} + \Omega_{p1}^{(-)} \approx \Omega_{p1}^{(+)} = U \exp[iK^+(0)z], \quad (35)$$

where U is a slowly varying function so that

$$\left[i\frac{\partial}{\partial z} + K^+(\omega)\right]\left[i\frac{\partial}{\partial z} + K^-(\omega)\right]\Omega_{p1} \simeq \exp[iK^+(0)z] \times [K^-(0) - K^+(0)]\left[i\frac{\partial}{\partial z} + K^+(\omega) - K^-(0)\right]U. \quad (36)$$

By substituting this form of the probe field Ω_{p1} into the propagation equations (12) and (13), we can obtain [63]

$$i\frac{\partial U}{\partial \xi} - \frac{1}{2}K_2^+\frac{\partial^2 U}{\partial \eta^2} - \chi \exp(-\alpha^+\xi)|U|^2 U = 0, \quad (37)$$

$$\Omega_{p2}(z,t) = W^+(0)\Omega_{p1}(z,t) = W^+ U \exp(iK_0^+ z), \quad (38)$$

with $\xi = z$, $\eta = t - z/V_g$, where $\alpha^+ = \text{Im}[K_0^+]$, $V_g = 1/K_1^+$, and K_2^+ denote the absorption coefficient, group velocity, and group-velocity dispersion, respectively.

$K_j^+ = j[\partial^j K^+(\omega)/\partial\omega^j]_{\omega=0}$ $(j = 1,2)$, $K^+(\omega)$ and $W^+(0)$ are given by Eqs. (28) and (29), and

$$\chi = \left[|A|^2 + \frac{|Ad_1+1|^2}{|\Omega_{c1}|^2} + \frac{|d_3 - A(|\Omega_{c1}|^2 - d_1 d_3)|^2}{|\Omega_{c1}|^2|\Omega_{c2}|^2}\right]K_0^+, \tag{39}$$

with $A = K_0^+/\kappa_{01}$. Equation (37) has complex coefficients and generally does not allow soliton solutions. However, as we show in Fig. 3, for the present system, practical parameters can be found so that α^+ may be made small, i.e., $\exp(-\alpha^+ L) \simeq 1$, and the imaginary parts of the complex coefficients are much smaller than the corresponding real parts, which yield $K_2^+ = K_{2r}^+ + iK_{2i}^+ \simeq K_{2r}^+$ and $\chi = \chi_r + i\chi_i \simeq \chi_r$. By defining $u = U^+/U_0$, $\sigma = \eta/\tau_0$, and $s = \xi/L_D$, Eq. (37) can be written in the dimensionless form corresponding to the standard NLSE governing the pulsed probe fields evolution

$$i\frac{\partial u}{\partial s} - g_D\frac{\partial^2 u}{\partial \sigma^2} - g_{NL}|u|^2 u = 0, \tag{40}$$

where $L_D = 2\tau_0^2/|K_{2r}^+|$ is dispersion length. In addition, we have assumed L_D is equal to L_{NL}, i.e., the balance of dispersion and nonlinearity, in order to favor the formation of a soliton, where $L_{NL} = 1/(U_0^2|\chi_r|)$ is the nonlinear length, with $2U_0 = (1/\tau_0)(2|K_{2r}^+|/|\chi_r|)^{1/2}$ being the typical Rabi frequency of the probe fields. Dimensionless coefficients of Eq. (40) are given by $g_D = \text{sign}(K_{2r}^+)$ and $g_{NL} = \text{sign}(\chi_r)$, respectively. Equation (40) is the well-known NLSE that is completely integrable and allows bright and dark soliton solutions, depending on the sign of $g_D g_{NL}$. When $g_D g_{NL} > 0$, one obtains the single bright soliton solution $u = \sqrt{2}\,\text{sech}(\sigma)\exp(-is)$ or, in terms of the probe fields,

$$\Omega_{p1}(z,t) = \frac{1}{\tau_0}\sqrt{\frac{|K_{2r}^+|}{|\chi_r|}}\,\text{sech}\left[\frac{1}{\tau_0}\left(t - \frac{z}{V_g^+}\right)\right] \times \exp\left[iK_0^+ z - i\frac{z}{L_D}\right], \tag{41}$$

$$\Omega_{p2}(z,t) = W^+(0)\frac{1}{\tau_0}\sqrt{\frac{|K_{2r}^+|}{|\chi_r|}}\,\text{sech}\left[\frac{1}{\tau_0}\left(t - \frac{z}{V_g^+}\right)\right] \times \exp\left[iK_0^+ z - i\frac{z}{L_D}\right], \tag{42}$$

which describe both probe fields $p1$ and $p2$ that have the same waveform propagating with common slow group velocity V_g^+. When $g_D g_{NL} < 0$, one obtains the single dark soliton solution

$$\Omega_{p1}(z,t) = \frac{1}{\tau_0}\sqrt{\frac{K_{2r}^+}{\chi_r}}\tanh\left[\frac{1}{\tau_0}\left(t - \frac{z}{V_g^+}\right)\right] \times \exp\left[iK_0^+ z - i\frac{z}{L_D}\right], \tag{43}$$

$$\Omega_{p2}(z,t) = W^+(0)\frac{1}{\tau_0}\sqrt{\frac{K_{2r}^+}{\chi_r}}\tanh\left[\frac{1}{\tau_0}\left(t - \frac{z}{V_g^+}\right)\right] \times \exp\left[iK_0^+ z - i\frac{z}{L_D}\right]. \tag{44}$$

Checking our assumption that leads to Eqs. (37)–(40) is indeed practical. Below, we give a practical example for a realistic $GaAs/Al_xGa_{1-x}As$ SQD system, with $\gamma_1 = \gamma_2 = 0.054$ meV, $\gamma_3 = 3.5 \times 10^{-3}\gamma_1$, and $\kappa_{01} \simeq \kappa_{01} = 3.4 \times 10^6$ cm^{-1} meV. Besides, taking $\Delta_1 = 3.1\gamma_1$, $\Delta_2 = 12\gamma_1$, $\Delta_3 = -0.05\gamma_1$, $|\Omega_{c1}| = |\Omega_{c2}| = 90\gamma_1$, and $\tau_0 = 300$ fs, we have $\chi = \chi_r + i\chi_i = (1.97 + 0.024i) \times 10^{-24}$ μm^{-1} s^2, and $K_2^+ = K_{2r}^+ + iK_{2i}^+ = (14.5 + 0.42i) \times 10^{-26}$ μm^{-1} s^2. Clearly, for all complex coefficients, the imaginary parts are indeed much smaller than their corresponding real parts. At the same time, we obtain $\alpha^+ = 0.000\,72$ μm^{-1}, $L_D = L_{NL} = 1.23$ μm. With these parameters, the standard NLSE in Eq. (40) with $g_D g_{NL} > 0$ is well characterized, and hence the existence of bright solitons in the SQD system is supported. The propagating velocity of the soliton is given by

$$V_g \simeq 4.3 \times 10^{-2} c, \tag{45}$$

which means that the optical soliton pairs propagate with the matched, slow propagating velocities in comparison with the light speed c in vacuum. With these parameter values, in Fig. 4(a), we show the result of numerical simulation on the soliton wave shape $|\Omega_{p1}/U_0|$ versus dimensionless time t/τ_0 and distance $z/(2L_D)$ with the full complex coefficients by

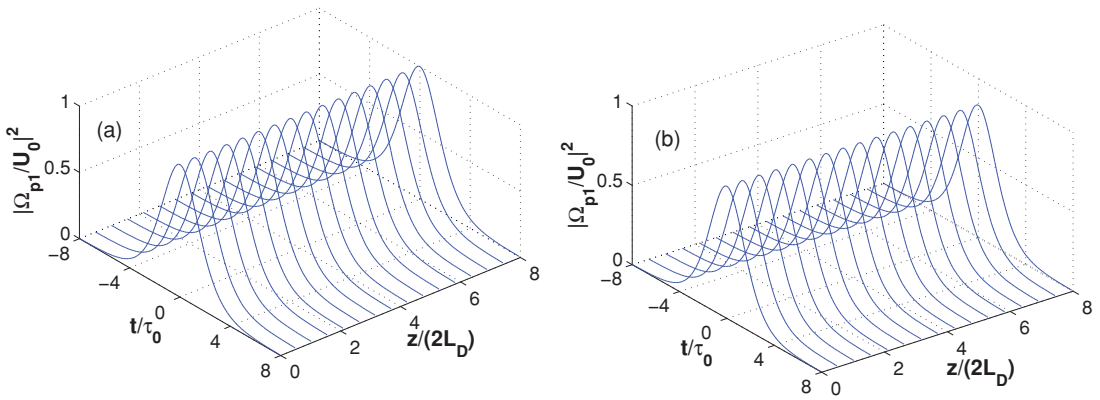

FIG. 4. (Color online) Surface plot of the probe intensity $|\Omega_{p1}/U_0|$ versus dimensionless time t/τ_0 and distance $z/(2L_D)$ obtained by numerically solving Eq. (37) without neglecting the imaginary part of coefficients with (a) $\gamma_3 = 3 \times 10^{-3}\gamma_1$, (b) $\gamma_3 = 4 \times 10^{-3}\gamma_1$. Other parameters in (a) and (b) are the same, which are given in the main text.

taking Eq. (41) as an initial condition. One can find that, in this case, the soliton is fairly stable during propagation without absorption. The result of numerical simulation shows excellent agreement with the exact soliton solution in Eq. (41). However, when the decay rate for the biexciton coherence increases, the bright soliton intensity reduces in a short propagation distance, as shown in Fig. 4(b). The results of Fig. 4(b) can be explained as follows: The degree of the induced transparency is determined by both γ_3 and $|\Omega_{c1}|$, and the biexciton coherence can be destroyed due to the increasing decay rate. Note that, although the destructive interference here resembles that of an atomic system, the biexciton coherence itself is a direct result of many particle Coulomb correlations and can thus lead to behaviors qualitatively different from those of an atomic system [55].

The collision property between two solitons is one of the most intriguing aspects in soliton dynamics. With the same parameter values as in Fig. 4(a), we have also investigated the collision feature between two bright optical solitons in the present SQD system by using numerical simulations. Figure 5 shows the waveforms for two different solitons with an initial separation for the same soliton amplitude and out of phase. In this case, the two solitons exhibit repulsive interaction. From Fig. 5, one can find that two solitons walk into each other in an initial stage and then separate from each other while recovering their initial waveforms. In addition, the spacing increases with distance monotonically due to the repulsive interaction. More interestingly, as the appropriate phase (position), a repulsive or attractive interaction can be realized in the collision [1,2], leading to a modulation or switching in a Mach-Zehnder configuration when the phase-shifted soliton interferes with another reference soliton [64]. Thus, we may provide more practical opportunities to implement all-optical switching and electro-optical modulated solid-state devices due to the flexibility in the semiconductor quantum structures [45].

It should be noted that we have neglected the contributions due to the time derivative terms $\mathcal{O}(\partial/\partial t)$ in deriving the nonlinear term (39). These contributions can lead to significant propagation effects at large propagation distances. For instance, the first-order time derivative will give an additional group-velocity correction [1], whereas other terms will contribute the high-order nonlinear and dispersion effects on the evolution of the pulsed probe fields. In order to study the influence of high-order nonlinear and dispersion effects, we must go beyond the standard NLSE, i.e., Eq. (40). By a detailed calculation, we rewrite Eq. (40) as

$$i\frac{\partial u}{\partial s}+\frac{\partial^2 u}{\partial \sigma^2}+|u|^2u+i \times\left[\theta_0 u-\theta_1\frac{\partial |u|^2u}{\partial\sigma}-\theta_2 u\frac{\partial |u|^2}{\partial\sigma}-\theta_3\frac{\partial^3 u}{\partial\sigma^3}\right]-\theta_4\frac{\partial u}{\partial\sigma}=0, \tag{46}$$

where the dimensionless coefficients in Eq. (46) are given by $\theta_j = 2L_D/L_j$ $(j = 0,1,2,3,4)$ with $L_0 = 1/\mathrm{Im}K_0^+$, $L_1 = \tau_0^3\chi_r/(B_{1r}K_{2r}^+)$, $L_2 = -\tau_0^3\chi_r/(B_{2r}K_{2r}^+)$, $L_3 = 6\tau_0^3/K_{3r}$, and $L_4 = \tau_0/K_{1i}$ the characteristic lengths of linear absorption, nonlinear dispersion, delay in nonlinear refractive index, third-order dispersion, and differential absorption, respectively. The expression of $K_{0,1r,2r,3r}$ is determined by Eq. (29). B_{jr} $(j = 1,2)$ represent the real part of B_j and the explicit expression B_j has been given in the Appendix. If the parameters of the system are chosen to make L_j $(j = 0,1,2,3,4)$ much larger than L_D, i.e., $\theta_j \ll 1$, the fourth and fifth terms in Eq. (46) can be taken as a perturbation. Under this condition, Eq. (46), when these perturbation contributions are neglected, reduced to the NLSE given in Eq. (40). With the same parameter values, in Fig. 8 we have plotted the coefficients θ_j $(j = 0,1,2,3,4)$ as functions of pulse duration τ_0. From Fig. 6, we found that with the above set of parameters and for longer pulse duration, i.e., $\tau_0 \geqslant 280$ fs, the linear and differential absorptions presented by θ_0 and θ_4 become relatively important [as shown in Fig. 6(a)]. Correspondingly, the effects due to the nonlinear dispersion, delay in nonlinear refractive index, and third-order dispersion represented by θ_1, θ_2, and θ_3 become negligible [as shown in Fig. 6(b)]. Thus, Eq. (40) is sufficiently accurate for pulse duration $\tau_0 \geqslant 280$ fs. If one reduces the pulse durations of the probe fields, the relative importance of these two groups of effects will be reversed.

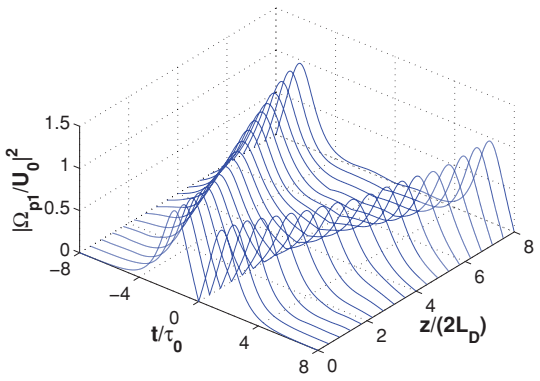

FIG. 5. (Color online) Surface plot of the solitary wave intensity $|\Omega_{p1}/U_0|^2$ versus dimensionless time t/τ_0 and distance $z/(2L_D)$ for the collision between two solitons by solving Eq. (37) with $\gamma_3 = 3\times10^{-3}\gamma_1$. Other parameters are the same as in Fig. 4(a).

We perform additional numerical simulations starting directly from Eqs. (1)–(9) and (12) without using any approximation. Figure 7(a) is propagation of $z = 4$ μm for the probe field intensity $|\Omega_{p1}/U_0|^2$, with Eq. (41) as the input condition. One can find that, except for small ripples appearing on its peak due to higher-order dispersions and high-order nonlinear effects that have not been included, the optical solitons produced here are rather stable as expected. We also show in Fig. 7(b) the simulation result of the collision between two bright optical solitons with the same initial condition as in Fig. 5. One can see again that the result is in a great agreement with the results shown in Fig. 5 and, thus, the full model in Eqs. (4)–(6) and (12) supports nearly shape-preserving soliton propagation.

Note that, by using the above parameters, it is easy to show that $W^+(0) \simeq 1$. Then, we can obtain $\Omega_{p1}(z,t) \simeq \Omega_{p2}(z,t)$. Thus, we have obtained a slowly propagating optical soliton pair with almost completely matched amplitude, waveform, and propagating velocity. This kind of matched slow optical soliton pairs not only are of theoretical importance but also may be double (due to the two

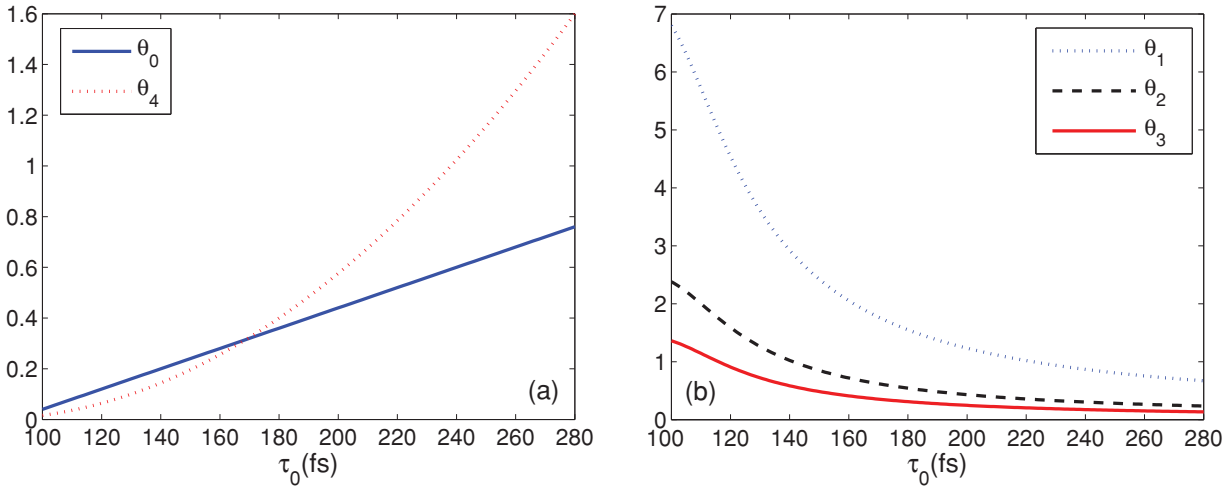

FIG. 6. (Color online) The coefficients θ_j ($j = 0,1,2,3,4$) versus pulse width τ_0: (a) θ_0 and θ_4, (b) θ_1, θ_2, and θ_3.

different carrier frequencies) the capacity for the applications of well-characterized and distortion-free slow optical wave packets in high fidelity optical buffers, transmission lines, switches, quantum information storage, and quantum computation [1,2].

In order to further demonstrate the formation and evolution of the matched slow optical soliton pairs in the SQD system and check their stabilities, we show in Fig. 8 the analytical solutions of Eqs. (37) and (38) (dashed lines) and the full numerical solutions (solid lines) obtained by directly integrating Eqs. (1)–(9) and (12) without using any approximations. In Fig. 8, we also show the numerical solutions without including nonlinear terms (dotted lines). We should note that the initial conditions used in the numerical calculations are $z = 0$ and $t = 0$, $\Omega_{p1}(0,t)/U_0 = \Omega_{p2}(0,t)/U_0 = \mathrm{sech}(t/\tau_0)$. Two features of Fig. 8 are most noteworthy. First, each curve contains two indistinguishable traces, representing the perfectly matched slow optical soliton pairs. Second, the curves without nonlinear terms exhibit severe pulse spreading as expected. The results of Fig. 8 indicate that the biexciton coherence plays a major role and also clearly validates the significance and importance of our theory.

IV. DISCUSSION AND CONCLUSION

Before conclusion, we give a brief discussion on the required threshold optical power density to support stable soliton propagation. In the parameter regime for the fundamental bright soliton discussed above, the flux of energy of the probe optical field associated with a single bright soliton is given by the Poynting vector integrated over the cross section of the quantum well sample: $P = \iint dS(\mathbf{E}_p \times \mathbf{H}_p) \cdot \mathbf{e}_z$, where $\mathbf{e}_z$ is the unit vector in the propagation direction. In leading-order approximation, the field is transverse and one has $\mathbf{E}_p = (E_{p1} + E_{p2},0,0)$, then $\mathbf{H}_p = (0, H_{p1} + H_{p2},0)$ with $H_{pj} = \varepsilon_0 c n(\omega_{pj}) E_{pj}$ ($j = 1,2$), where $n(\omega_{pj})$ is the refractive index of the probe field at frequency ω_{pj}. It is easy to obtain the average flux of energy over a carrier-wave period

$$\bar{P} = \bar{P}_{\max} \mathrm{sech}^2\left[\frac{1}{\tau_0}\left(t - \frac{z}{V_g^+}\right)\right], \tag{47}$$

where the peak power reads as

$$\begin{aligned}\bar{P}_{\max} &= 2\varepsilon_0 c S_0 [n(\omega_{p1})|\mathcal{E}_{p1}|^2 + n(\omega_{p2})|\mathcal{E}_{p2}|^2] \\ &= \frac{4\hbar^2 \varepsilon_0 c S_0 K_{2r}^+}{\tau_0^2 \chi_r}\left[\frac{n(\omega_{p1})}{|\mu_{10}|^2} + \frac{n(\omega_{p1})(W^+)^2}{|\mu_{20}|^2}\right],\end{aligned} \tag{48}$$

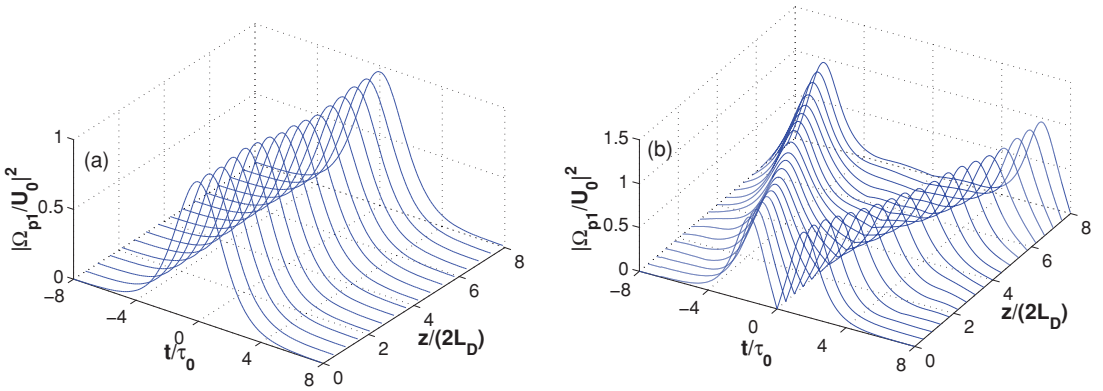

FIG. 7. (Color online) (a) Surface plot of the solitary wave intensity $|\Omega_{p1}/U_0|^2$ versus dimensionless time t/τ_0 and distance $z/(2L_D)$ obtained by numerically integrating Eqs. (1)–(9) and (6). (b) Collision between two solitons. The parameters are set $\gamma_4 = \gamma_5 = \gamma_6 = \gamma_1$; other parameters are the same as in Fig. 4(a).

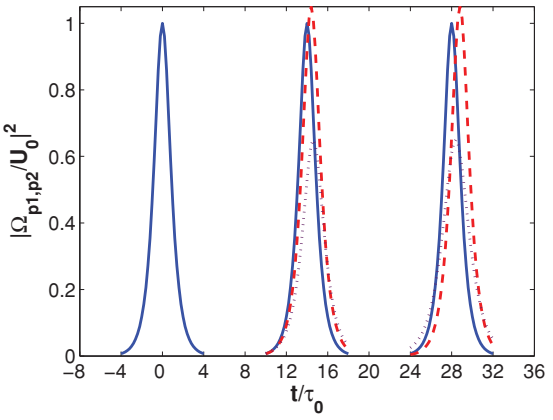

FIG. 8. (Color online) Comparison of analytical solutions of Eqs. (40)–(42) (dashed lines) and the full numerical solutions (solid lines) obtained by directly integrating Eqs. (4)–(9) and (12) and (13) without using any approximations. The dotted lines are numerical solutions without including nonlinear terms. Each curve contains three indistinguishable traces, that is, $|\Omega_{p1}/U_0|^2$ and $|\Omega_{p2}/U_0|^2$. The parameters are the same as in Fig. 4.

with S_0 the cross-section area of the sample and $n(\omega_{pj})$ the refractive index of the jth probe field. We find that the peak power is directly proportional to the dispersion coefficient K_{2r}^{+} and inversely proportional to the square of the pulse width τ_0 as well as the self-phase modulation coefficient χ_r. By using the above numerical values of the system parameters and taking $S_0 = \pi \times 10^{-7}$ cm^2, we obtain $\bar{P}_{\max} = 47$ mW. Thus, we argue that very low input power is needed for generating a matched optical soliton pair in our SQD system. This is drastically different from the conventional optical soliton generation technique using optical fibers where laser pulses are needed to reach very high peak power in order to bring out the nonlinear effect needed for soliton formation.

We should note that the slowly varying envelope approximation (i.e., $\partial\Omega_{p1,p2}/\partial z \ll k_{p1,p2}$, $\partial\Omega_{p1,p2}/\partial t \ll \omega_{p1,p2}\Omega_{p1,p2}$) has been used for obtaining Eqs. (12) and (13) governing the evolution of the probe fields. In the case of the soliton solutions given above, such a condition corresponds to $\lambda_{p1,p2} \ll V_g\tau_0$ and $\omega_{p1,p2}\tau_0 \gg 1$. It is easy to check that the soliton solutions presented above satisfy these conditions. With the parameter values of the system specified in Sec. III, we have $\omega_{p1}\,\omega_{p2} \approx 2 \times 10^{15}$ Hz, $\lambda_{p1}\,\lambda_{p2} = 0.94\ \mu$m, and $V_g = 4.3 \times 10^{-2}c$. Since $\tau_0 = 300$ fs, we obtain $V_g\tau_0 = 3.87\ \mu$m and $\omega_{p1,p2}\tau_0 = 0.6 \times 10^3$, which validate fairly well the slowly varying envelope approximation condition. In addition, with the parameters provided above, we have the spatial length of the soliton $L_s \equiv V_g^{+}\tau_0 = 3.87\ \mu$m, the disperion length $L_D = 1.23\ \mu$m, and the absorption length $L_A = 2/\alpha^{+} \approx 2.8 \times 10^3\ \mu$m. In the setup for possible experiments, light can be injected along the z axis (the wave vector $k_{p1,p2,c1,c2}$ parallel to the plane of the SQD structure), and we consider a transverse magnetically polarized probe field incident with respect to the growth direction (y axis). This configuration is preferred due to a relatively long propagation distance (on the order of millimeters), larger than the dispersion length L_D and spatial length of the soliton L_s, to observe the soliton formation.

It is worth to point out that there are some relevant works on solitons and breathers in semiconductors [65,66]. For example, in Ref. [65], Adamashvili *et al.* considered the condition of self-induced transparency (SIT) in multilevel quantum dots, in which a single optical field with 2π or 0π area is needed to induce the required coherent pulse propagation, while here we use four input optical fields, i.e., two cw control and two probe fields, which construct the destructive interference channels via biexciton coherence and lead to a giant suppression of the linear absorption and simultaneously an enhancement of SPM coefficient for the probe fields. Furthermore, the degree of the destructive interference is determined by both the decay rate for the biexciton coherence γ_3 and the amplitude of the cw control fields $|\Omega_{c1,c2}|$. More interestingly, we stress that, under suitable conditions, it is possible to generate a stable soliton pair using only one input, i.e., $\Omega_{p2}(0.0) = 0$, but with a lower efficiency [67]. This generally requires that a multiple-single-channel-induced-transparency based on four-wave-mixing process be operative [68]. If this is achievable, the soliton formation and propagation follow as described above.

In conclusion, we have proposed a scheme to produce a pair of matched slow optical solitons via biexciton coherence in a solid-state SQD structure. By coupling two cw control fields to a biexciton state, the linear as well as the nonlinear dispersions are dramatically enhanced simultaneously with the absorptions of two pulsed probe fields being almost suppressed under appropriate conditions in the medium. In order to obtain the corresponding nonlinear evolution equations, we have employed the perturbation approach to the density matrix equations. We have also shown that detrimental distortions of probe fields due to strong dispersion effects under weak driving conditions can be well balanced by SPM effects, resulting in a pair of optical solitons with matched group velocity and amplitude. Aside from this, we demonstrated that there exist parameter regimes in which the optical soliton pair can propagate stably through the present system with slow group velocities ($V_g \sim 10^{-2}c$), in contrast to optical fibers where the group velocity of the supported soliton is close to the speed of light in vacuum.

ACKNOWLEDGMENTS

This work was supported by the National Natural Science Foundation of China (NSFC) under Grants No. 11074036, No. 10874050, No. 10975054, and No. 91021011 and by the National Fundamental Research Program of China Grant No. 2007CB936300.

APPENDIX: EXPRESSION OF THE COEFFICIENTS IN Eq. (46)

The expressions of the coefficients in Eq. (46) are given by

$$B_1 = \frac{-(\kappa_{01}D_{c2} + \kappa_{02}D_{c1}) + G}{2D}(Q_1 + Q_1^{*}) - \frac{|D_{c1}|^2 + |D_{c2}|^2 + |\Omega_{c1}|^2\left(d_1^2 + |\Omega_{c2}|^2\right) + |\Omega_{c2}|^2\left(d_2^2 + |\Omega_{c1}|^2\right)}{2(\kappa_{01}D_{c2} + \kappa_{02}D_{c1})D}\chi, \quad \text{(A1)}$$

$$B_2 = \frac{-(\kappa_{01}D_{c2}+\kappa_{02}D_{c1})+G}{2D}(2Q_1+Q_1^*) - \frac{|D_{c1}|^2+|D_{c2}|^2+|\Omega_{c1}|^2\left(d_1^2+|\Omega_{c2}|^2\right)+|\Omega_{c2}|^2\left(d_2^2+|\Omega_{c1}|^2\right)}{4(\kappa_{01}D_{c2}+\kappa_{02}D_{c1})D}\chi, \quad \text{(A2)}$$

with $D_{cj} = D_{cj}(\omega)|_{\omega=0}$ $(j = 1,2)$, $D = D(\omega)|_{\omega=0}$, $G = G(\omega)|_{\omega=0}$, and

$$Q_1 = -\frac{d_3}{2D\kappa_{01}\kappa_{02}}\left[d_2\left(\frac{1}{V_g}-\frac{1}{c}\right)+\left(\frac{-(\kappa_{01}D_{c2}+\kappa_{02}D_{c1})+G}{2D}-\frac{1}{c}\right)\right]^* + \frac{(\kappa_{01}D_{c2}+\kappa_{02}D_{c1})+G}{2D\kappa_{01}\kappa_{02}}\left(\frac{1}{V_g}-\frac{1}{c}\right)$$
$$+\frac{1}{2\kappa_{01}\kappa_{02}D}\left[-d_3\left(\frac{d_2}{V_g}-\frac{d_2}{c}-\frac{-(\kappa_{01}D_{c2}+\kappa_{02}D_{c1})+G}{2D}-\frac{1}{c}\right)+|\Omega_{c1}|^2\left(\frac{1}{V_g}-\frac{1}{c}\right)-\kappa_{01}\kappa_{02}\frac{|\Omega_{c1}|^2d_2+|\Omega_{c2}|^2d_1}{2D}\right]^*, \quad \text{(A3)}$$

where the asterisk represents a complex conjugate.

[1] Yu. S. Kivshar and G. P. Agrawal, *Optical Solitons: From Fibers to Photonic Crystals* (Academic, San Diego, 2003).
[2] G. P. Agrawal, *Nonlinear Fiber Optics*, 3rd ed. (Academic, New York, 2001); A. Hasegawa and M. Matsumoto, *Optical Solitons in Fibers* (Springer, Berlin, 2003).
[3] R.-K. Lee, Elena A. Ostrovskaya, Yuri S. Kivshar, and Y. Lai, Phys. Rev. A **72**, 033607 (2005).
[4] D. V. Skryabin, A. V. Yulin, and A. I. Maimistov, Phys. Rev. Lett. **96**, 163904 (2006).
[5] W.-X. Yang, Y.-Y. Lin, T.-D. Lee, R.-K. Lee, and Yuri S. Kivshar, Opt. Lett. **35**, 3207 (2010).
[6] M. Fleischhauer, A. Imamoglu, and J. P. Marangos, Rev. Mod. Phys. **77**, 633 (2005).
[7] H. Schmidt and A. Imamoglu, Opt. Lett. **21**, 1936 (1996).
[8] S. E. Harris and L. V. Hau, Phys. Rev. Lett. **82**, 4611 (1999).
[9] M. D. Lukin and A. Imamoglu, Phys. Rev. Lett. **84**, 1419 (2000).
[10] D. F. Phillips, A. Fleischhauer, A. Mair, R. L. Walsworth, and M. D. Lukin, Phys. Rev. Lett. **86**, 783 (2001).
[11] D. Petrosyan and G. Kurizki, Phys. Rev. A **65**, 033833 (2002).
[12] Y. Wu and X. Yang, Phys. Rev. A **71**, 053806 (2005).
[13] Y. Wu, L. L. Wen, and Y. F. Zhu, Opt. Lett. **28**, 631 (2003).
[14] D. Petrosyan and Yuri P. Malakyan, Phys. Rev. A **70**, 023822 (2004).
[15] S. Rebić, D. Vitali, C. Ottaviani, P. Tombesi, M. Artoni, F. Cataliotti, and R. Corbalán, Phys. Rev. A **70**, 032317 (2004).
[16] Y. Wu and L. Deng, Phys. Rev. Lett. **93**, 143904 (2004).
[17] X.-T. Xie and M. A. Macovei, Phys. Rev. Lett. **104**, 073902 (2010).
[18] G. Huang, K. Jiang, M. G. Payne, and L. Deng, Phys. Rev. E **73**, 056606 (2006).
[19] X. J. Liu, H. Jing, and M. L. Ge, Phys. Rev. A **70**, 055802 (2004).
[20] Y. Wu and X. X. Yang, Appl. Phys. Lett. **91**, 094104 (2007).
[21] L. Deng, M. G. Payne, G. Huang, and E. W. Hagley, Phys. Rev. E **72**, 055601(R) (2005).
[22] W.-X. Yang, A.-X. Chen, L.-G. Si, K. Jiang, X. Yang, and R.-K. Lee, Phys. Rev. A **81**, 023814 (2010).
[23] J. Faist, F. Capasso, C. Sirtori, K. West, and L. N. Pfeiffer, Nature (London) **390**, 589 (1997).
[24] G. B. Serapiglia, E. Paspalakis, C. Sirtori, K. L. Vodopyanov, and C. C. Phillips, Phys. Rev. Lett. **84**, 1019 (2000).
[25] M. C. Phillips, H. Wang, I. Rumyantsev, N. H. Kwong, R. Takayama, and R. Binder, Phys. Rev. Lett. **91**, 183602 (2003).
[26] L. Silvestri, F. Bassani, G. Czajkowski, and B. Davoudi, Eur. Phys. J. B **27**, 89 (2002).
[27] V. Yannopapas, E. Paspalakis, and N. V. Vitanov, Phys. Rev. B **80**, 035104 (2009).
[28] S. M. Ma, H. Xu, and B. S. Ham, Opt. Express **17**, 14902 (2009).
[29] S. Marcinkevicius, A. Gushterov, and J. P. Reithmaier, Appl. Phys. Lett. **92**, 041113 (2008).
[30] A. Imamoglu and R. J. Ram, Opt. Lett. **19**, 1744 (1994).
[31] C. R. Lee, Y. C. Li, F. K. Men, C. H. Pao, Y. C. Tsai, and J. F. Wang, Appl. Phys. Lett. **86**, 201112 (2005).
[32] M. D. Frogley, J. F. Dynes, M. Beck, J. Faist, and C. C. Phillips, Nat. Mater. **5**, 175 (2006).
[33] R. Atanasov, A. Hache, J. L. P. Hughes, H. M. van Driel, and J. E. Sipe, Phys. Rev. Lett. **76**, 1703 (1996).
[34] P. C. Ku, F. Sedgwick, C. J. Chang-Hasnain, P. Palinginis, T. Li, H. Wang, S. W. Chang, and S. L. Chuang, Opt. Lett. **29**, 2291 (2004).
[35] E. Paspalakis, M. Tsaousidou, and A. F. Terzis, Phys. Rev. B **73**, 125344 (2006).
[36] P. I. Tamborenea and H. Metiu, Phys. Lett. A **240**, 265 (1998).
[37] J. H. Li, Phys. Rev. B **75**, 155329 (2007).
[38] P. Lunnemann and J. Mork, Appl. Phys. Lett. **94**, 071108 (2009).
[39] J. H. Wu, J. Y. Gao, J. H. Xu, L. Silvestri, M. Artoni, G. C. La Rocca, and F. Bassani, Phys. Rev. Lett. **95**, 057401 (2005).
[40] A. Joshi and M. Xiao, Appl. Phys. B **79**, 65 (2004).
[41] C. Z. Ning, Phys. Rev. Lett. **93**, 187403 (2004).
[42] N. C. Nielsen, S. Linden, J. Kuhl, J. Förstner, A. Knorr, S. W. Koch, and H. Giessen, Phys. Rev. B **64**, 245202 (2001).
[43] H. Sun, S. Gong, Y. Niu, S. Jin, R. Li, and Z. Xu, Phys. Rev. B **74**, 155314 (2006).
[44] C. Zhu and G. Huang, Phys. Rev. B **80**, 235408 (2009).
[45] H. C. Liu and F. Capasso, *Intersubband Transitions in Quantum Wells: Physics and Device Applications* (Academic, New York, 2000).
[46] B. Krummheuer, V. M. Axt, and T. Kuhn, Phys. Rev. B **65**, 195313 (2002).
[47] J. Förstner, C. Weber, J. Danckwerts, and A. Knorr, Phys. Rev. Lett. **91**, 127401 (2003).
[48] A. Krügel, V. M. Axt, T. Kuhn, P. Machnikowski, and A. Vagov, Appl. Phys. B **81**, 897 (2005).
[49] W.-X. Yang, J.-M. Hou, and R.-K. Lee, Phys. Rev. A **77**, 033838 (2008).

[50] W.-X. Yang and R.-K. Lee, Europhys. Lett. **83**, 14002 (2008).
[51] W.-X. Yang, J.-M. Hou, Y. Y. Lin, and R.-K. Lee, Phys. Rev. A **79**, 033825 (2009).
[52] D. Gammon, E. S. Snow, B. V. Shanabrook, D. S. Katzer, and D. Park, Science **273**, 87 (1996).
[53] K. Brunner, G. Abstreiter, G. Böhm, G. Tränkle, and G. Weimann, Phys. Rev. Lett. **73**, 1138 (1994).
[54] W. Langbein, P. Borri, U. Woggon, V. Stavarache, D. Reuter, and A. D. Wieck, Phys. Rev. B **69**, 161301 (2004).
[55] V. M. Axt and S. Mukamel, Rev. Mod. Phys. **70**, 145 (1998).
[56] I. Waldmüller, J. Förstner, S.-C. Lee, A. Knorr, M. Woerner, K. Reimann, R. A. Kaindl, T. Elsaesser, R. Hey, and K. H. Ploog, Phys. Rev. B **69**, 205307 (2004).
[57] S. M. Sadeghi and J. Meyer, Phys. Rev. A **58**, 2534 (1998).
[58] S. M. Sadeghi and H. M. van Driel, Phys. Rev. B **63**, 045316 (2001).
[59] M. O. Scully and M. S. Zubairy, *Quantum Optics* (Cambridge University Press, Cambridge, England, 1997), Chap. 5, p. 168.
[60] G. Chen, T. H. Stievater, E. T. Batteh, X. Li, D. G. Steel, D. Gammon, D. S. Katzer, D. Park, and L. J. Sham, Phys. Rev. Lett. **88**, 117901 (2002).
[61] W. Langbein, P. Borri, U. Woggon, V. Stavarache, D. Reuter, and A. D. Wieck, Phys. Rev. B **69**, 161301(R) (2004).
[62] M. Paillard, X. Marie, P. Renucci, T. Amand, A. Jbeli, and J. M. Gerard, Phys. Rev. Lett. **86**, 1634 (2001).
[63] H. A. Haus and W. S. Wong, Rev. Mod. Phys. **68**, 423 (1996).
[64] S. R. Friberg, Opt. Lett. **16**, 1484 (1991).
[65] G. T. Adamashvili, C. Weber, A. Knorr, and N. T. Adamashvili, Phys. Rev. A **75**, 063808 (2007).
[66] F. Biancalana, S. B. Healy, R. Fehse, and E. P. O'Reilly, Phys. Rev. A **73**, 063826 (2006).
[67] Y. Wu, Phys. Rev. A **71**, 053820 (2005).
[68] Y. Wu and X. Yang, Phys. Rev. A **70**, 053818 (2004).